PHASE IMAGING VIA SPARSE CODING IN THE COMPLEX DOMAIN BASED ON HIGH-ORDER SVD AND NONLOCAL BM3D TECHNIQUES

Vladimir Katkovnik[1], *Karen Egiazarian*[1], *José Bioucas-Dias*[2]

[1]Signal Processing Department,
Tampere University of Technology, {vladimir.katkovnik, karen.eguiazarian}@tut.fi
[2]Instituto de Telecomunicações, Instituto Superior Técnico, ULisboa, Portugal, bioucas@lx.it.pt

ABSTRACT

The paper addresses interferometric phase image estimation, that is, the estimation of phase modulo-2π images from sinusoidal 2π-periodic and noisy observations. These degradation mechanisms make interferometric phase image estimation a challenging problem. We tackle this challenge by reformulating the true estimation problem as a sparse regression in the complex domain. Following the standard procedure in patch-based image restoration, the image is partitioned into small overlapping square patches. BM3D algorithm equipped with high order SVD (HOSVD) is used to form complex domain frames suitable to sparse representations of the complex-valued data. HOSVD applied to the groups of BM3D data enables the design of spatially variant and data adaptive orthonormal complex domain transforms. The effectiveness of the new sparse coding based approach to interferometric phase estimation, termed ***In**terferometric **PHASE** via **B**lock matching and **H**igh order **SVD*** (InPHASE-BHS) is illustrated in a series of simulation experiments where it outperforms the state-of-the-art.

Index Terms— Phase imaging, interferometric phase estimation, phase unwrapping, sparse regression, BM3D, high order SVD.

1. INTRODUCTION

In this paper, we are focussed on a wide class of phase imaging problems concerning wave field sensing, reconstruction, and manipulation. In particular, a monochromatic coherent wave field defined in a given domain X is modeled by complex amplitude $u = ae^{j\varphi}$, where a and φ, are, respectively, the amplitude and phase images of the wave field, defined on X, and both can be time and space varying. In modern technology and science the phase and wave field imaging are very popular and well established technique for high-accuracy measuring, recording and reconstructing 2D and 3D objects. The areas of applications are numerous varying from astronomy and engineering to medicine and biology (e.g., [1], [2]). In engineering the phase and wave field sensing methods serve for nondestructive testing/control and precise measurements (e.g., [3], [4], [5]). In medicine and biology phase measurements are exploited in microscopy and coherent tomography, using, for instance, Fourier phase microscopy. We wish to mention also such developments as the phase based registration of brain dynamics, express blood tests, measurement of distribution of biological pigments and biological structures in body tissues, etc.

Thanks for funding to Academy of Finland, project no. 138207, 2011-2014, and Fundação para a Ciência e Tecnologia (FCT), Portuguese Ministry of Science and Higher Education, projects PEst-OE/EEI/0008/2013 and PTDC/EEI-PRO/1470/2012.

The topic of sparse and redundant representations of images given by intensities has attracted tremendous interest from the research community in the last ten years. This interest stems from the fundamental role that the low dimensional models play in many signal and image areas such as compression, restoration, classifications, and design of priors and regularizers, just to name a few [6], [7]. Real world images admit a sparse representation, *i.e*, given an image, there exists a basis consisting of a small number of items where it can be represented exactly or approximately with a very good accuracy. This ideal basis is a priory unknown and selected from a given set of potential bases (dictionary or dictionaries). To add yet more interest to this imaging techniques, the dictionaries yielding sparse representations may be learned from the data they represent. Dictionary learning is currently one of the hottest research topics in this area [6].

Sparse imaging can be viewed as a parametric approximation of signals with an adaptive basis selection, one of the classical topics in statistics. The modern popularity and success of sparse imaging are due to a wealth of new theoretical and algorithmic results, many of then borrowed from compressive sensing (CS), a closely related area, and the evidence that the developed formalism fits many important applications.

1.1. Related work

Recently in optics, sparse imaging in complex domain has become a subject of multiple applications. Complex-valued signals and operators are distinctive features of this development. Basic facts of the corresponding theory, algorithms, simulations as well as experimental demonstrations can be found in [8], where CS is used for subwavelength imaging thereby overcoming the diffraction limitations. In the works concerning the complex-valued data, the estimation of the phase is the most challenging problem, which in the case of sparse representations include the design of the phase dictionary. Part of these difficulties are a direct consequence of the periodic map linking the phase to be estimated and the observations.

Work [9] attacks CS wave field in hyperspectral imaging using a quadratic penalization for phase used jointly with the TV penalty for the complex-valued wave field. The results obtained are step forward in this area. Works [10] and [11] introduce separate sparse modeling for the phase and the amplitude and formulates the wave field inference in a multiobjective optimization framework. The results obtained with proposed methodologies are state-of-the-art.

1.2. Proposed work

In this paper, we are focussed on designing adaptive synthesis and analysis frames (termed dictionaries in sparse representation jargon)

based on the BM3D technique (Block Matching three dimensional filtering) [12], to model the wave field. The image is partitioned into small overlapping rectangular patches and the vector corresponding to each patch is modeled as a sparse linear combination of vectors, termed atoms, taken from a dictionary. For each patch, a group of similar patches is collected from a pre-defined neighborhood and stacked together forming a 3D array. A 3D analysis frame is then applied to the array. The obtained spectral coefficients are hard/soft-thresholded and the collaboratively filtered patches synthesized with a synthesis frame. This process is repeated over the entire image and the obtained overlapped filtered patches are aggregated in the final image estimate. See [12] for further details.

We modify the BM3D as it is presented in [12] in two ways. First, patching and grouping of similar patches are applied to complex-valued variables. Second, we adopt third order HOSVD (see, *e.g.*, [13], [14], [15], [16]) as analysis frame. After applying HOSVD to the 3D groups, we obtain complex valued groupwise spectrums of the complex-valued data and three orthonormal complex-valued bases/transforms: two for each variable of 2D patches and the third one for the length variable of the group. Thus, instead of the fixed real-valued analysis frames originally proposed in BM3D [12], we obtain adaptive group dependent and complex-valued frames, where the phases and magnitude are linked in a very special way. This new technique can be understood as a generalization for the complex domain of our BM3D-SAPCA algorithm [17], where SVD is used for design of 2D orthonormal bases for patches, and also of HOSVD-BM3D proposed in [18], where 3D-SVD is used for design of the real-valued orthonormal transforms for all three variables in BM3D groups.

Links between BM3D technique and the design of the frames for sparse redundant approximations are discussed in [20]. For the developed algorithms we obtain similar type complex-valued frames. Details of this development are out of context of this paper.

Our preliminary results provide evidence that the proposed complex domain sparse codings work amazingly well even without the Wiener filtering usually used in BM3D as the second stage of the algorithm.

1.3. Organization

The paper is organized as follows. Section 2 presents the proposed wave field estimation algorithm including its main steps: grouping, analysis using HOSVD, thresholding, inverse HOSVD, and aggregation. Section 3 presents results with simulated data providing evidence of the effectiveness and competitiveness of the proposed methodology. Finally, Section 4 ends the paper with a few concluding remarks and pointers to future work.

2. ALGORITHM DEVELOPMENT

Let us assume that the observed data $z : X \to \mathbb{C}$, where $X \subset \mathbb{Z}^2$ is 2D grid of size $N \times N$, is modeled as

$$z(x) = a(x)e^{j\varphi(x)} + n(x),$$

where $x \in X$, $u(x) = a(x)e^{j\varphi(x)}$ is the true complex valued image and $n(x) = n_I(x)+jn_Q(x)$ is complex-valued zero-mean Gaussian circular white noise of variance σ^2 (i.e., $n_I(x)$ and $jn_Q(x)$ are zero-mean independent Gaussian random variables with variance $\sigma^2/2$). In addition, we also assume that the collection of random variables $\{n(x), x \in X\}$ is independent.

With the objective of formulating treatable phase imaging inverse problems, most approaches follow a two-step procedure: in the first step, an estimate of the true phase in the interval $[-\pi, \pi)$, the so-called *principal phase values*, or *wrapped phase*, or *interferometric phase*, is inferred from noisy wrapped observations; in the second step, the true phase is inferred from the interferometric phase estimate obtained in the first step. The latter procedure is known as phase unwrapping and corresponds to the addition of an integer number of 2π multiples to the estimated interferometric phase [21], [22]. In this paper, our primary objective is the estimation of the interferometric phase from noisy observations.

Given the phase φ, the corresponding interferometric phase is defined as $\varphi_{2\pi} = \mathcal{W}(\varphi)$, where $\mathcal{W} : \mathbb{R} \to [-\pi, \pi)$, $\varphi_{2\pi} = [(\varphi+\pi) \mod 2\pi] - \pi$ [21]. With these definitions in place, the interferometric phase estimation problem is to estimate the image $\varphi_{2\pi}$ from the observed image z.

Following the standard procedure in patch-based image restoration, the $N \times N$ images, noisy $\mathbf{z} \equiv \{z(x), x \in X\}$ and true $\mathbf{u} \equiv \{u(x), x \in X\}$, are partitioned into small overlapping rectangular/square patches of size $N_1 \times N_2$. Then, following closely [12], we implement the following 5 steps: grouping, collaboratively filtering via HOSVD transform, hard-thresholding of HOSVD spectrum, inverse HOSVD transform, and aggregation of the overlapping patch estimates. Compared with [12], we have two major differences: a) the images are complex; b) the transform used to carry out the 3D filtering is the HOSVD, which brings groupwise data adaptiveness not present in [12]. In the ensuing sections, we detail the above steps.

2.1. Grouping

Let $\mathbf{P}_x \equiv \{z(y), y \in \mathcal{P}_x \subset X\}$ denote a rectangular image patch of size $N_1 \times N_2$ defined on the domain $\mathcal{P}_x$, where the index $x \in X$ corresponds to the upper-left pixel of the patch. Define also the set $\mathcal{S}_r \subset X$

$$\mathcal{S}_r \equiv \{x \in X : d(\mathbf{P}_x - \mathbf{P}_r) \leq \tau_r \sigma^2\}, \tag{1}$$

where $d(\mathbf{P}_x - \mathbf{P}_r)$ denotes the Euclidean distance between patches $\mathbf{P}_x$ and $\mathbf{P}_r$, and τ_r is a parameter controlling the maximum distance between any two patches with indices in $\mathcal{S}_r$. The number of elements of $\mathcal{S}_r$ is denoted by J_r.

The matched noisy patches $\mathbf{P}_x$, for $x \in \mathcal{S}_r$ are stacked to form a 3D array of size $N_1 \times N_2 \times J_r$, denoted by $\mathbf{Z}^r$.

2.2. High order SVD

The 3D groups $\mathbf{Z}^r \in \mathbb{C}^{N_1 \times N_2 \times J_r}$ can be understood as a tensor of the dimension $N_1 \times N_2 \times J_r$. The elements of this tensor can be expressed as $\mathbf{Z}^r_{l_1,l_2,l_3}$with $l_1 \in \{1, ..., N_1\}$, $l_2 \in \{1, ..., N_2\}$ and $l_3 \in \{1, ..., J_r\}$. Following a recent trend in multichannel image restoration and in video [19], [18], we use multilinear algebra techniques to treat the group $\mathbf{Z}^r$ as a whole 3D entity and thereby taking into account the correlation of variations inside and between patches.

There are a number of tensor decompositions of which we mention TUCKER3 and PARAFAC [13]. In this paper we are focussed on the HOSVD (TUCKER3) transform which allows to represent a given group-tensor, $\mathbf{Z}^r$, in the form

$$\mathbf{Z}^r = \mathbf{S}^r \times_1 \mathbf{T}_{1,r} \times_2 \mathbf{T}_{2,r} \times \mathbf{T}_{3,r}, \tag{2}$$

where $\mathbf{T}_{1,r} \in \mathbb{C}^{N_1 \times N_1}$, $\mathbf{T}_{2,r} \in \mathbb{C}^{N_2 \times N_2}$ and $\mathbf{T}_{3,r} \in \mathbb{C}^{N_{J_r} \times N_{J_r}}$ are orthonormal transform matrices, $\mathbf{S}^r \in \mathbb{C}^{N_1 \times N_2 \times J_r}$ is the so-called *core tensor*, and symbols $\times_1$, $\times_2$, and $\times_3$ stand for the products of the corresponding modes (variables). The matrix transforms $\mathbf{T}_{1,r}$, $\mathbf{T}_{2,r}$, and $\mathbf{T}_{3,r}$ acts , respectively, on variables l_1, l_2, and l_3.

2.3. Thresholding

In the standard SVD, the spectral matrix is diagonal and its diagonal elements are singular values of the matrix. Often, a given matrix is well approximated by a small number of singular components corresponding to the dominant singular values. These *truncated SVD* based approximations have been extensively used in signal and image processing both to carry out denoising and to obtain low rank approximation of the original matrices.

HOSVD applied to the complex-valued data gives complex-valued orthonormal transform matrices $\mathbf{T}_{1,r}$, $\mathbf{T}_{2,r}$, and $\mathbf{T}_{3,r}$ and a complex-valued core matrix $\mathbf{S}^r$. Contrarily to the 2D case, the core tensor $\mathbf{S}$ is not diagonal [13]. However, as show the experiments, in our application, a small number of tensor components with large energy dominate the group representation. Thus, assuming that the smaller elements of $\mathbf{S}$ are linked to noise and not to essential components of the signal, the standard elementwise hard-thresholding filtering of $\mathbf{S}^r$ can be used in the form

$$\widehat{\mathbf{S}}^r = \text{hard}(\mathbf{S}^r, \delta_r), \tag{3}$$

where hard$(\cdot)$ is the well known hard threshold function defined as hard$(z, \delta_r) = 0$ if $|z| \leq \delta_r$ and hard$(z, \delta_r) = z$ if $|z| > \delta_r$. The notation hard$(\mathbf{S}^r, \delta_r)$ is to be understood in the componentwise sense.

Following [24], we select as the universal threshold $\delta_r = \eta_r \sigma \sqrt{2 \log N_1 N_2 J_r}$, where η_r is an algorithm parameter selected from experiments. After the thresholding the filtered group data (tensor) is reconstructed using the formula (2) as

$$\widehat{\mathbf{U}}^r = \widehat{\mathbf{S}}^r \times_1 \mathbf{T}_{1,r} \times_2 \mathbf{T}_{2,r} \times \mathbf{T}_{3,r}. \tag{4}$$

2.4. Aggregation and wave field reconstruction.

After the thresholding step, each of the 3D groups $\widehat{\mathbf{U}}^r$, for $r \in X$, contains J_r stacked local patch estimates $\widehat{\mathbf{P}}_{x \in \mathcal{S}_r}$ of the true patches. We remark that due to the patch overlapping and grouping process, the set of patches contained in the 3D groups $\widehat{\mathbf{U}}^r$, for $r \in X$, provides an overcomplete representation of the estimated image $\widehat{\mathbf{u}}$. In order to compute and estimate of $\mathbf{u}$, define $\widehat{u}_{r,y}(x)$ as the estimate of $u(x)$ provided by patch $y \in X$ if $y \in \mathcal{S}_r$ and $x \in \mathcal{P}_y$ and $\widehat{u}_{r,y}(x) = 0$ otherwise. With these definition in place, we compute the estimate of $u(x)$ as

$$\widehat{u}(x) = \frac{\sum_{r \in X} \sum_{y \in \mathcal{S}_r} \widehat{u}_{r,y}(x)}{\sum_{r \in X} \sum_{y \in \mathcal{S}_r} \mathcal{I}_{\mathcal{P}_y}(x)}, \tag{5}$$

where $\mathcal{I}_{\mathcal{P}_y}$ stands for the indicator of set $\mathcal{P}_y$. It is worth mentioning that the denominator of (5) is always grater of equal to 1 because all image pixels are covered at least by a patch. In practice, for most pixels we have $\sum_{r \in X} \sum_{y \in \mathcal{S}_r} \mathcal{I}_{\mathcal{P}_y}(x) > 1$ because at least one patch containing x was collaboratively used in more than one group.

Finally, the reconstructed interferometric phase and the magnitude is computed as follows:

$$\hat{a}(x) = \text{abs}(\widehat{u}(x)), \quad \widehat{\varphi}_{2\pi} = \arg(\widehat{u}(x)), \quad x \in X. \tag{6}$$

3. RESULTS

In this section, we present a series of results using simulated data to illustrate the competitiveness and effectiveness of the proposed algorithm termed ***In**terferometric **PHASE** via **B**lock matching and **H**igh order **SVD*** (InPHASE-BHS).

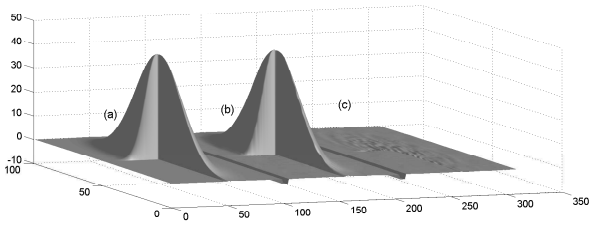

Fig. 1. Absolute truncated Gaussian phase: true (a), reconstruction (b), errors (c).

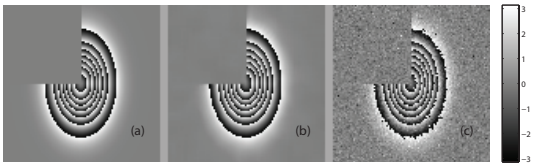

Fig. 2. Interferometric truncated Gaussian phase: true (a), reconstruction (b), measurements (c).

Based on the true interferometric phase $\varphi_{2\pi}$ and on the estimated interferometric phase estimate $\widehat{\varphi}_{2\pi}$, we define the peak signal-to-noise ratio (PSNR) as

$$\text{PSNR} = 10 \log_{10} \frac{4N^2\pi^2}{||\mathcal{W}(\widehat{\varphi}_{2\pi} - \varphi_{2\pi})||_F^2} [dB],$$

where $\mathcal{W}$ is the wrapping operator. We also unwrap the estimated interferometric phase with the PUMA algorithm [22] and obtain the estimates of the absolute phase φ, in particular to evaluate the quality and reliability of the interferometric estimate provided InPHASE-BHS.

From the estimated phase $\widehat{\varphi}_{2\pi}$ of the true phase φ, define the set of image pixels with error no larger than 2π, i.e., $I := \{l_1, l_2 : |\widehat{\varphi}(l_1, l_2) - \varphi(l_1, l_2)| \leq \pi$ and, based on this set, define the number of errors larger than 2π (NELP) and the peak signal-to-noise for the absolute phase

$$\text{PSNR}_a = 10 \log_{10} \frac{4N^2\pi^2}{||\widehat{\varphi}_I - \varphi_I)||_F^2} [dB],$$

where the notation φ_I stands for the restriction of φ to I. That is, PSNR$_a$ is computed with respect to the set I. Because the unwrapping is defined apart from a constant 2π multiple, when computing the set I, we identify the constant 2π multiple that minimizes l. We remark that the performance indicators NELP and PSNR$_a$, in addition to the information they give about the quality of the estimated true phase, are also a characterization of the denoising algorithm, as the success of the unwrapping depends crucially on the quality of the interferometric phase.

In all experiments the patch size is $N_1 = N_2 = 8$, the size of groups is limited to $J_r \leq 41$, and the threshold parameters (scale parameter of for the hard-thresholding) is set to $\eta_r = 2$. InPHASE-BHS is compared with window Fourier Transform (WFT) algorithm using the codes publicly available [1]. In WFT the windowed Fourier transform of z is calculated and hard-thresholded. The inverse windowed Fourier transform is applied in order to obtain the estimate of

[1] WFT-WFT-http://www.mathworks.fr/matlabcentral/fileexchange/24892

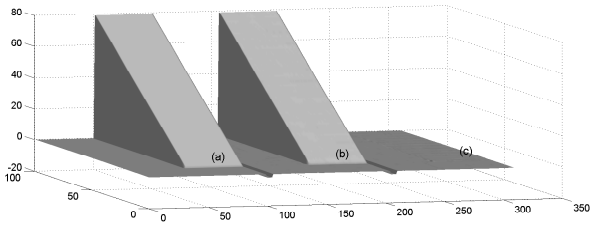

Fig. 3. Absolute shear plane phase: true (a), reconstruction (b), errors (c).

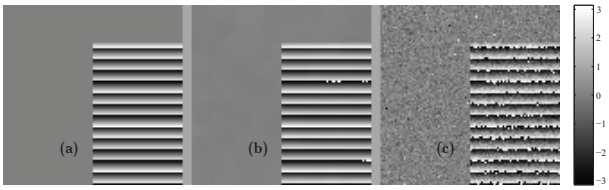

Fig. 4. Interferometric shear plane phase: true (a), reconstruction (b), measurements (c).

y, $\varphi_{2\pi}$ and a. WFT estimates were obtained with the following parameters: size of the windows $\sigma_x = \sigma_y = 4$; threshold for the windowed Fourier transform $th = 3\sigma$; frequency interval $[-\pi, \pi]$; and sampling interval 0.1. This setting was determined experimentally aiming at optimal performance for the set of experiments considered. We remark that this setting yields considerable better results than that recommenced in [23] (i.e., $\sigma_x = \sigma_y = 10$ and $[-\pi/2, \pi/2]$). We use WFT for comparison as the current state-of-the-art for the interferometric phase reconstruction.

In our MATLAB implementation of InPHASE-BHS we use the tool box tptool 090831 for HOSVD transform [2], modified version of the BM3D algorithm [3] and the PUMA algorithm for phase unwrapping [4]. All the algorithms ran on a personal computer equipped with a Core i7-3770 CPU and 8.00 GB RAM.

Figs 1 and 2 shows, respectively absolute phase and interferometric phase estimation results for a truncated Gaussian phase surface and where the magnitude is set to $a = 1$ and the noise variance is set to $\sigma = 0.5$. Figs 3-4 show results similar to Figs 1-2 for a shear plane. We remark that the interferometric absolute phase estimation in these two examples is a an extremely hard problem owing to the the presence of discontinuities. Any attempt to directly low pass filtering the noisy data $\mathbf{z}$ would destroy interferometric phase information coded in the $\mathbf{z}$ what would compromise the success of any posterior unwrapping.

Table I shows the performance indicators for the truncated Gaussian and shear planes phase surfaces and for $\sigma \in \{0.3, 0.5, 0.7, 0.9\}$ corresponding to increasing levels of difficulty from moderate to very hard. The numerical advantage of the proposed algorithm is about 3 dB for the truncated Gaussian phase and about 7 dB for shear plane phase. Thus, numerically and visually the InPHASE-BHS algorithm demonstrate a great deal of advantage over the current state-of-the-art WFT algorithm.

Finally, Fig. 5 shows the histogram of the number of active (used) elements of the core (spectral) tensor per group in the shear plane surface and for $\sigma = 0.5$. The total number of the groups

[2]tptool-090831- http://www.tp-control.hu/index.php/About

[3]BM3D-http://www.cs.tut.fi/~foi/GCF-BM3D/

[4]PUMA-http://www.lx.it.pt/~bioucas/code.htm

Table 1. PSNR for interferometric and absolute phase reconstruction. The values in the brackets were obtained by WFT algorithm.

Phase	σ	PSNR (dB)	PSNR$_a$(dB)	NELP
Gauss Trunc	0.3	43.83 (40.29)	43.83 (40.29)	0 (0)
	0.5	40.15 (36.71)	40.15 (36.71)	0 (0)
	0.7	37.59 (34.26)	37.59 (34.37)	6 (10)
	0.9	35.56 (32.79)	35.81 (32.79)	0 (0)
Shear Plane	0.3	48.91 (40.67)	48.91 (40.67)	0 (0)
	0.5	44.44 (37.07)	44.44 (37.07)	0 (0)
	0.7	41.45 (34.13)	41.45 (34.13)	0 (0)
	0.9	39.14 (33.24)	39.14 (33.24)	0 (0)

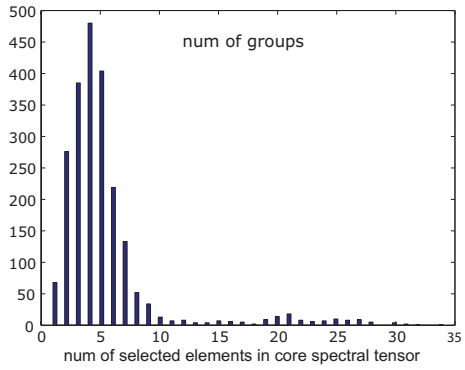

Fig. 5. Histogram of the number of active elements of the core (spectral) tensor per group in the shear plane surface and for $\sigma = 0.5$.

for the image is 2209. Given that the 3D group-tensor has size 8x8x41=2624 and that in most cases the number of the active elements in the group varies between 2 and 6, we conclude, therefore, that the representation of the groups is extremely sparse.

4. CONCLUDING REMARKS

This paper introduced InPHASE-BHS, an effective algorithm for interferometric phase image estimation, that is, the estimation of phase modulo-2π images from sinusoidal 2π-periodic and noisy observations. The true problem was recast as the estimation of the true complex valued image via sparse representation of the complex image patches on learned HOSVD analysis/synthesis. The sparse representations, also termed sparse coding, are computed by the orthogonal matching. These transforms are learned via HOSVD factorization of BM3D groups. The filtering of the HOSVD spectrum is produced using componentwise hard-thresholding. In a series of experiences with simulated data, InPHASE-BHS produced systematically better estimates than the state-of-the-art with a significant advantage. We highlight the InPHASE-BHS ability to preserve the interferometric information coded in discontinuities and areas of high phase rate, which is the essential requirement for the success of phase unwrapping.

As future work, we will research on the use of different 3D array decomposition as well as matrix representations of 3D data with 2D arrays allowing the use of the standard SVD. The Wiener filtering will be developed as an additional tool in order to improve the phase imaging in the complex domain. Another area where we will develop our approach concerns more complex observations mechanisms in which we do not have direct access to the noisy exponential data as it for instance for example in various optical interferometric applications.

5. REFERENCES

[1] *Principles of Adaptive Optics*, 3rd ed., CRC Press, 2010.

[2] L. Wang and H. Wu, *Biomedical Optics: Principles and Imaging*, John Wiley & Sons, Inc., 2007.

[3] Th. Kreis, *Handbook of Holographic Interferometry*, Wiley-VCH, Berlin, 2005.

[4] B. Kress and P. Meyrueis, *Applied Digital Optics: From Micro-Optics to Nanooptics*, John Wiley & Sons, Inc., 2009 .

[5] A. Patil and P. Rastogi, "Moving ahead with phase," *Optics and Lasers in Engineering*, vol. 45, no. 2, pp. 253-257, 2007.

[6] M. Elad, *Sparse and Redundant Representations: from Theory to Applications in Signal and Image Processing*, Springer, 2010.

[7] J.-L. Starck, F. Murtagh, and J. M. Fadili, *Sparse Image and Signal Processing: Wavelets, Curvelets, Morphological Diversity*, Cambridge University Press, 2010.

[8] S. Gazit, A. Szameit, Y. C. Eldar, M. Segev, "Super-resolution and reconstruction of sparse sub-wavelength images, " *Optics Express* vol. 17, pp. 23920–23946, 2009 .

[9] Z. Xu and E. Lam ,"Image reconstruction using spectroscopic and hyperspectral information for compressive terahertz imaging", *Journal of the Optical Society of America A*, vol. 27, no. 7, pp. 1638–1646, 2010.

[10] V. Katkovnik and J. Astola, "High-accuracy wavefield reconstruction: decoupled inverse imaging with sparse modeling of phase and amplitude", *Journal of the Optical Society of America A*, vol. 29, pp. 44–54, 2012.

[11] V. Katkovnik and J. Astola, "Phase retrieval via spatial light modulator phase modulation in 4f optical setup: numerical inverse imaging with sparse regularization for phase and amplitude", *Journal of the Optical Society of America A*, vol. 29, pp. 105–116, 2012.

[12] K. Dabov, A. Foi, V. Katkovnik, and K. Egiazarian, "Image denoising by sparse 3D transform-domain collaborative filtering", *IEEE Transactions on Image Processing*, vol. 16, no. 8, pp. 2080–2095, 2007.

[13] L. De Lathauwer, B. De Moor, J. Vandewalle, "A multilinear singular value decomposition", *SIAM Journal on Matrix Analysis and Applications*, vol. 21, pp. 1253–1278, 2000.

[14] L. Tucker, "Some mathematical notes on three-mode factor analysis, Psychometrika", vol. 31, pp. 279–311, 1966.

[15] P. Kroonenberg, J. De Leeuw, "Principal component analysis of three-mode data by means of alternating least squares algorithms", *Psychometrika*, vol. 45, no. 1, pp. 69–97, 1980.

[16] J. Kruskal, "Three-way arrays: rank and uniqueness of trilinear decomposition, with application to arithmetic complexity and statistics", *Annals of Statistics*, vol. 18, pp. 95–138, 1977.

[17] A. Foi, V. Katkovnik, and K. Egiazarian, "Pointwise shape-adaptive DCT for high-quality denoising and deblocking of grayscale and color images", *IEEE Transactions on Image Processing*, vol. 16, no. 5, pp. 1395–1411, 2007.

[18] A. Rajwade, A. Rangarajan and A. Banerjee, "Image denoising using the higher order singular value decomposition", *IEEE Transactions on Pattern Analysis and Machine Intelligence*, vol. 35, no. 4, pp. 849–862, 2013.

[19] A. Rajwade, A. Rangarajan, and A. Banerjee, "Using the higher order singular value decomposition for video denoising," *Energy Minimization Methods in Computer Vision and Pattern Recognition*, pp. 344–354, 2011

[20] A. Danielyan, V. Katkovnik, and K. Egiazarian, " BM3D frames and variational image deblurring, " *IEEE Transactions on Image Processing*, vol. 21, pp. 1715–1728, 2012.

[21] D. Ghiglia and M. Pritt, *Two-Dimensional Phase Unwrapping: Theory, Algorithms, and Software*, Wiley, 1998.

[22] J. M. Bioucas-Dias and G. Valadão, "Phase unwrapping via graph cuts, " *IEEE Transactions on Image Processing*, vol. 16, no. 3, pp. 698–709, 2007.

[23] Q. Kemao, *Windowed Fringe Pattern Analysis*, SPIE, Bellingham, Whashington, 2013.

[24] D. Donoho and I. Johnstone, "Ideal spatial adaptation by wavelet shrinkage," *Biometrika*, vol. 81, pp. 425–455, 1993.